Journal of Inflammation Research

Dovepress
Taylor & Francis Group

Open Access Full Text Article

ORIGINAL RESEARCH

Banxia-Xiexin Decoction Ameliorates Colitis-Associated Colorectal Cancer by Modulating Inflammatory Responses and the Complement and Coagulation Cascade Pathway

Qiang Chen, Maoxu Wang, Wei Shi, Yinan Liu, Liying Wang, Yuegang Zhao, Zhidong Qiu, Ye Qiu, Xuelian Dong

Institute of College of Pharmacy, Changchun University of Chinese Medicine, Changchun, 130117, People's Republic of China

Correspondence: Xuelian Dong, Email dongxl@ccucm.edu.cn

Purpose: Colitis-associated colorectal cancer (CAC), a subtype of colorectal cancer arising from chronic colonic inflammation, currently lacks specific therapeutic agents. Banxia-Xiexin decoction (BXD), a traditional Chinese medicine, is clinically used for gastritis and ulcerative colitis; however, its efficacy and underlying mechanisms in CAC remain unclear. This study aimed to evaluate the therapeutic potential of BXD against CAC and elucidate its molecular mechanisms.

Methods: A CAC mouse model was induced using azoxymethane/dextran sulfate sodium (AOM/DSS). Mice received BXD at low, medium, and high doses (0.95, 1.9, or 3.8 g/kg/day) by oral gavage from day 21 to day 70, or sulfasalazine (0.6 g/kg/day) as a positive control. Therapeutic efficacy was evaluated by disease index (DI), histopathology, and inflammatory cytokine levels (TNF-α, IL-6, IL-1β, IFN-γ). Metabolomic profiling and proteomic analysis were performed to identify altered metabolic pathways and differentially expressed proteins (DEPs). Key pathway-related genes were validated by qRT-PCR.

Results: BXD treatment significantly alleviated clinical symptoms, attenuated colonic inflammation, and reduced both tumor number and size compared with the model group. Inflammatory cytokines were markedly decreased. Metabolomics revealed modulation of amino acid and glycerophospholipid metabolism, while proteomics identified DEPs enriched in the complement and coagulation cascades. Expression of key proteins (C3,Fgg, Cpb2, Cfh) and corresponding mRNAs was reversed by BXD.

Conclusion: BXD may ameliorate CAC by modulating inflammatory responses and glycerophospholipid metabolism, with particular involvement of the complement and coagulation cascades. These findings provide mechanistic insight into the potential anti-CAC effects of BXD and support its further investigation for clinical application.

Keywords: Banxia-Xiexin decoction, colitis-associated colorectal cancer, serum metabolomics, proteomics, complement and coagulation cascades

Introduction

Ulcerative colitis and Crohn's disease are inflammatory bowel diseases that elevate the risk of colitis-associated colorectal cancer (CAC), a subtype with higher mortality rates compared to sporadic colorectal cancer. As the incidence of CAC rises over time,[1] effective management strategies are increasingly crucial. Current clinical approaches to manage colonic inflammation and mitigate CAC risk include the use of aminosalicylic acids, immunomodulators, antioxidants, antitumor biological agents, and other chemical therapeutics.[2] Recent studies have identified key molecular pathways involved in inflammation-associated tumorigenesis, such as the NF-κB pathway, Wnt/β-catenin signaling, PGE2/COX-2, IL-6/STAT3, the IL-23/Th17 axis, TNF-α signaling, and oxidative stress induced by chronic inflammation.[3,4] These pathways represent crucial links between persistent inflammation and cancer development. Additionally, gut microbiota dysbiosis and abnormal metabolic pathways have emerged as potential risk factors for CAC.[5]

Received: 25 August 2025
Accepted: 20 October 2025
Published: 30 October 2025

Despite the widespread use of chemical agents, their effectiveness in treating CAC remains limited due to severe side effects, incomplete targeting of underlying mechanisms, and failure to restore gut microbiota balance.[6] Although probiotics show potential in reducing postoperative complications in colorectal cancer (CRC) patients, definitive evidence of their protective role against CAC is lacking. Clinical trial data on probiotic use in CAC treatment are also insufficient.[7] While current treatments primarily focus on these molecular pathways, alternative therapies, particularly those from Traditional Chinese Medicine (TCM), are emerging as complementary options. TCM has attracted attention for its potential to modulate intestinal inflammation and microbiota. Classical TCM prescriptions have shown efficacy in inhibiting CAC by restoring intestinal microbial balance, enhancing the gut barrier, and alleviating inflammation. For example, Quxie capsule has been demonstrated to improve CAC by promoting beneficial microorganisms like Lactobacillus, Bifidobacterium, and Faecalibacterium, while reducing harmful species like Bacteroides and Aspergillus fumigatus.[8] Similarly, Qingchang Wenzhong decoction alleviates CAC by promoting intestinal fibrosis, reinforcing the mucosal barrier, and regulating inflammatory signaling pathways such as IL-17, NF-κB, and TLR4.[9] In recent years, proteomic and metabolomic techniques have been employed to analyze colon tissues, blood, and other biological samples from CAC models. These studies suggest that alterations in protein expression and metabolic pathways may be associated with enhanced inflammatory and immune responses, contributing to CAC development.[10–12] Several differentially expressed proteins and metabolites identified in these studies may serve as potential CAC biomarkers.

Banxia-Xiexin Decoction (BXD), a classical TCM formula originating from the Shang Han Lun (Treatise on Febrile Diseases), consists of seven botanical ingredients (Table S1). Traditionally, it has been used to harmonize the liver and spleen, balance cold and heat, and dissolve masses. In modern clinical practice, it is widely used to treat conditions such as gastroenteritis, inflammatory bowel disease, diarrhea, functional dyspepsia, and gastroesophageal reflux.[13,14] Recent experimental studies have indicated that water-soluble extracts of BXD exert therapeutic effects in oxazolone-induced colitis murine models by reducing the mRNA expression levels of IL-5 and IL-13 in colonic tissues, thereby alleviating colitis symptoms.[15] Wang et al demonstrated, through network pharmacology and in vitro/in vivo experiments, that BXD targets the PI3K/AKT/mTOR pathway, induces ferritinophagy-mediated iron accumulation and reactive oxygen species activation, and triggers ferroptosis, significantly inhibiting colorectal cancer growth.[16] Similarly, Luo et al revealed that BXD reshapes the gut microbiota in a DSS-induced ulcerative colitis mouse model by increasing the abundance of beneficial bacteria, such as Muribaculaceae, Akkermansia, and Lactobacillus, while reducing potentially pathogenic genera like Faecalibaculum and Alloprevotella.[17] These findings collectively suggest that BXD exerts multifaceted bioactivities, including anti-inflammatory, antitumor, and microbiota-modulating effects, which may be relevant to CAC prevention or treatment.

Although previous studies have demonstrated that BXD and its major phytochemicals can modulate inflammation, immune function, and lipid metabolism,[18,19] no reports to date have directly linked BXD to the regulation of the complement–coagulation–glycerophospholipid metabolic axis. Given the well-established role of this axis in promoting chronic inflammation, tumor progression, and metabolic dysregulation in CAC,[20,21] addressing this gap may advance our understanding of BXD's mechanisms. Therefore, in the present study, we established a murine model of CAC and conducted integrated colon tissue proteomics and serum metabolomics analyses to identify potential molecular targets and signaling pathways associated with BXD intervention. Candidate mechanisms were subsequently validated at the molecular level, aiming to provide a systematic mechanistic framework that supports the potential translational application of BXD in CAC management.

Materials and Methods

Chemicals and Reagents

Mouse ELISA kits for TNF-α, IL-6, IL-1β, and IFN-γ were obtained from Jiangsu Enzyme Immunity Industry Co., Ltd. (Jiangsu, China). Trizol reagent was purchased from Servicebio (Wuhan, China). The RevertAid First Strand cDNA Synthesis Kit was obtained from Thermo Fisher Scientific (Waltham, MA, USA). The ProteoMiner™ Protein Enrichment Small-Capacity Kit was purchased from Bio-Rad (Hercules, CA, USA). BSA was purchased from DAKO (Glostrup, Denmark). Antibodies against NF-κB was purchased from ABclonal Biotechnology Co., Ltd. (Wuhan, China).

IFN-γ antibody was purchased from Aibixin Biotechnology Co., Ltd. (Shanghai, China). HIF-1α antibody was purchased from Bioss Biotechnology Co., Ltd. (Beijing, China).

Plant Materials and Extraction

Pinellia ternata (Thunb). Breit, *Zingiber officinale* Rosc., *Scutellaria baicalensis* Georgi, *Coptis chinensis* Franch, *Ziziphus jujuba* Mill., *Glycyrrhiza uralensis* Fisch., and *Panax ginseng C.A*. Mey were purchased from Ji Lin Pharmacy (Jilin, China). All herbs were authenticated by Prof. Li-li Weng (Changchun University of Chinese Medicine). For the preparation of BXD, 83.3 g of mixed crude herbs were soaked in 2,000 mL of distilled water for 30 minutes and then decocted for an additional 30 minutes. The extract was filtered, and the filtrate was lyophilized to obtain a dry powder for further use.

UHPLC–MS/MS Conditions for Phytochemical Analysis

A total of 300 mg of the lyophilized BXD powder was extracted with 1,000 μL of methanol/water (4:1, v/v) containing an internal standard (2-chloro-L-phenylalanine, 10 μg/mL). Samples were sonicated in an ice-water bath for 5 min, incubated at –40 °C for 1 h, and centrifuged at 12,000 rpm for 15 min at 4 °C. The supernatants were filtered through a 0.22 μm membrane, and 100 μL aliquots from each sample were pooled to prepare quality control (QC) samples. All samples were stored at –80 °C until analysis. Chromatographic separation was performed on a Waters BEH C18 column (1.7 μm, 2.1×100 mm) using water (A) and acetonitrile (B) as the mobile phases, both containing 0.1% formic acid. The injection volume was 5 μL, with a flow rate of 0.4 mL/min, and the column temperature was maintained at 40 °C. The gradient elution program is shown in Table 1.

Mass spectrometry (MS) data were acquired using a Q Exactive mass spectrometer equipped with Xcalibur software in IDA mode (m/z range: 100–1,500; top three MS/MS per cycle). The settings were as follows: sheath gas, 30 arbitrary units; auxiliary gas, 10 arbitrary units; capillary temperature, 350 °C; full MS resolution, 70,000; MS/MS resolution, 17,500; normalized collision energy (NCE), 15/30/45; spray voltage, +5.5 kV (positive mode) and –4.0 kV (negative mode).

Animals and Experimental Design

Six-week-old male C57BL/6 mice (20 ± 2 g, SPF) were purchased from Liaoning Changsheng Biotechnology Co., Ltd. (License No. SCXK (Liao) 2020–0001). Animals were housed under controlled environmental conditions (22 ± 2 °C, 50 ± 10% relative humidity, 12 h light/dark cycle) with free access to standard chow and water. The animal experiment protocol was approved by the Animal Experiment Ethics Committee of Changchun University of Chinese Medicine (Approval No. 2023508) and conducted in accordance with the NIH Guidelines for the Care and Use of Laboratory Animals.

CAC Model Establishment and Treatment

Forty-eight 6-week-old male specific-pathogen-free (SPF) mice were randomly divided into six groups (n = 8/group): control (Control), model (Model), BXD low-dose (BXDL), BXD medium-dose (BXDm), BXD high-dose (BXDh), and

Table 1 Elution Gradient Program

Time (min)	Proportion of B Phase
0	5
3.5	15
6	30
6.5	30
12	70
12.5	70
18	100
25	100
26	5
30	5

positive control (ST). To induce CAC, all groups except the control were injected intraperitoneally with azoxymethane (AOM, 10 mg/kg; Sigma−Aldrich, USA), followed by a 7-day treatment with 2% dextran sulfate sodium (DSS; MP Biomedicals, Canada) in drinking water. After a 7-day recovery period, mice were treated with regular water for 14 days. The DSS cycle was repeated three times. The control group received saline injections and standard water. BXD dosage was normalized based on body surface area: BXDL (0.95 g/kg/day), BXDm (1.9 g/kg/day), and BXDh (3.8 g/kg/day), administered orally from day 29 to day 70. The ST group received sulfasalazine (0.6 g/kg/day) by oral gavage for the same period. All groups received an equal volume of saline as the vehicle. After six weeks of treatment, mice were sacrificed under CO_2 anesthesia, and tissues and serum were collected for further analysis.

Clinical Assessment of CAC

The severity of CAC was evaluated by two independent observers blinded to the treatment allocations. Starting from day 7 after AOM injection, body weight, stool consistency, coat condition, and the disease index (DI) were recorded weekly. Occult blood in the feces was detected using the o-toluidine method. The DI was scored as follows: 0 = normal feces; 2 = soft feces or occult blood; 4 = diarrhea or grossly bloody feces.

Histopathological Analysis

The colon was harvested, fixed in 4% paraformaldehyde, dehydrated through a graded ethanol series, cleared in xylene, embedded in paraffin, and sectioned at 5 μm thickness. Sections were stained with hematoxylin and eosin (HE) and examined under a light microscope for histopathological evaluation.

Detection of Serum Inflammatory Cytokines

Serum concentrations of IL-1β, IL-6, TNF-α, and IFN-γ were measured using commercial ELISA kits according to the manufacturers' instructions. Optical density was read at 450 nm, and cytokine levels were calculated based on standard curves generated for each assay.

Immunofluorescence Staining

Colon tissue sections were dewaxed in xylene and rehydrated through a graded ethanol series, followed by antigen retrieval using an appropriate retrieval buffer. After blocking with 5% BSA to prevent nonspecific binding, sections were incubated overnight at 4 °C with primary antibodies against HIF-1α, IFN-γ, and NF-κB. Subsequently, the sections were incubated with species-appropriate fluorescently labeled secondary antibodies at room temperature in the dark. Cell nuclei were counterstained with DAPI. Fluorescence microscopy was employed to observe the specific protein staining, and signal intensity was analyzed using ImageJ software.

Metabolomics Analysis

Fasting blood samples were collected in EDTA-coated vacutainer tubes and centrifuged at 1,500 × g for 15 minutes at 4°C. Plasma aliquots (150 μL) were stored at –80°C. For metabolomic analysis, plasma samples were thawed at 4°C, mixed with 400 μL of cold methanol/acetonitrile (1:1, v/v), and centrifuged at 14,000 × g for 20 minutes at 4°C. The supernatants were evaporated, reconstituted in 100 μL acetonitrile/water (1:1, v/v), and subjected to final centrifugation before LC-MS injection.

UHPLC (Vanquish, Thermo) coupled to Orbitrap was employed for analysis. HILIC separation was performed using a 2.1×100 mm ACQUITY UPLC BEH Amide 1.7 μm column (Waters, Ireland). The mobile phases were A: 25 mM ammonium acetate and 25 mM ammonium hydroxide in water; B: acetonitrile. The gradient was: 98% B (1.5 min), reduced to 2% (10.5 min), held (2 min), increased to 98% (0.1 min), followed by 3 minutes of re-equilibration. ESI source settings: Gas1 60, Gas2 60, CUR 30, source temp 600°C, ISVF ±5,500 V. MS range: m/z 80–1,200; resolution: 60,000; accumulation time: 100 ms. For auto MS/MS: m/z 70–1,200; resolution: 30,000; accumulation time: 50 ms. Pareto-scaled principal component analysis (PCA) was used to identify differential metabolites and pathways.

Proteomic Analysis

Total protein was extracted from colon tissues by grinding samples in liquid nitrogen, precipitating with cold 10% TCA/acetone (1:4, v/v) at −20°C for 4 hours, and washing with cold acetone. The pellets were lysed in buffer (8 M urea, 1% protease inhibitor cocktail), sonicated, and centrifuged at 12,000 × g for 10 minutes at 4°C. Protein concentration was determined using a BCA assay. For PTM experiments, specific inhibitors for acetylation and phosphorylation were added to the lysis buffer.

Protein samples were enzymatically digested and the resulting peptides separated by reversed-phase nano-UPLC (NanoElute, Bruker Daltonics). Peptides were analyzed on a timsTOF Pro 2 mass spectrometer in dia-PASEF mode. Raw data were processed using DIA-NN (v1.8) software and searched against the Mus musculus FASTA database with a 1% FDR cutoff. Differentially expressed proteins (DEPs) were identified by $P < 0.05$ and $|\text{fold change}| > 1.5$,and subjected to enrichment analysis.

RNA Extraction and Quantitative Real-Time Polymerase Chain Reaction (qRT-PCR)

Total RNA was isolated from colon tissues, reverse transcribed cDNA, which was then amplified via quantitative PCR. Cycling conditions: 95 °C for 30s, followed by 40 cycles of 95 °C for 15s, 60 °C for 30s. The $2^{-\Delta\Delta CT}$ method was used to calculate gene expression levels, with GAPDH serving as the internal control for comparison of CT values. Primer sequences are provided in Table 2.

Statistical Analysis

GraphPad Prism (v10.1.2) was utilized for data analysis and plotting. Results are expressed as mean values with standard error. Group differences were evaluated by one-way ANOVA followed by Tukey's multiple-comparisons test, with $p < 0.05$ considered statistically significant.

Results

Identification of Metabolites in BXD

The base peak intensity (BPI) chromatograms of BXD in positive (A) and negative (B) ionization modes are shown in Figure 1. A total of 67 primary metabolites were identified based on accurate mass and MS/MS fragmentation patterns, as summarized in Table 3 together with their physicochemical properties.

Quantitative determination, performed using calibration curves of authentic standards, revealed relatively high levels of several key constituents in BXD. The most abundant compounds included guanine (255.22 μg/g), trigonelline hydrochloride (189.79 μg/g), ginsenoside Rg1 (143.12 μg/g), liquiritin (95.95 μg/g), wogonin (51.85 μg/g), wogonoside (34.65 μg/g), berberine (29.94 μg/g), ginsenoside Rb3 (26.88 μg/g), uracil (24.50 μg/g), ginsenoside Rb2 (13.27 μg/g), uridine (6.91 μg/g), baicalin (5.80 μg/g), ginsenoside Rh3 (4.09 μg/g), ginsenoside Re (3.48 μg/g), ginsenoside Rg6 (3.03 μg/g), ginsenoside Rg2 (2.61 μg/g), palmatine chloride (1.96 μg/g), ginsenoside Ro (1.06 μg/g), and 6-gingerol (0.43 μg/g).

Table 2 The Primer Sequences

Gene	Primer Sequence (5′-3′)
M-GAPDH-F	CCTCGTCCCGTAGACAAAATG
M-GAPDH-R	TGAGGTCAATGAAGGGGTCGT
M-Cpb2-F	GCTCACAAGAACAACCGCTG
M-Cpb2-R	TGACGCACCTTTCTCACACC
M-C3-F	TTGTCCCCTTGAAGATCGGC
M-C3-R	TCATTCCTTCTGGCACGACC
M-Fgg-F	GATTTGGACACCTGTCGCCT
M-Fgg-R	CATAGTCCGCAGTGCTGGTT
M-Cfh-F	GGATCCACCACATGTGCCAA
M-Cfh-R	ATTTCCCTGTTGAGTCTCGGC

https://doi.org/10.2147/JIR.S562302

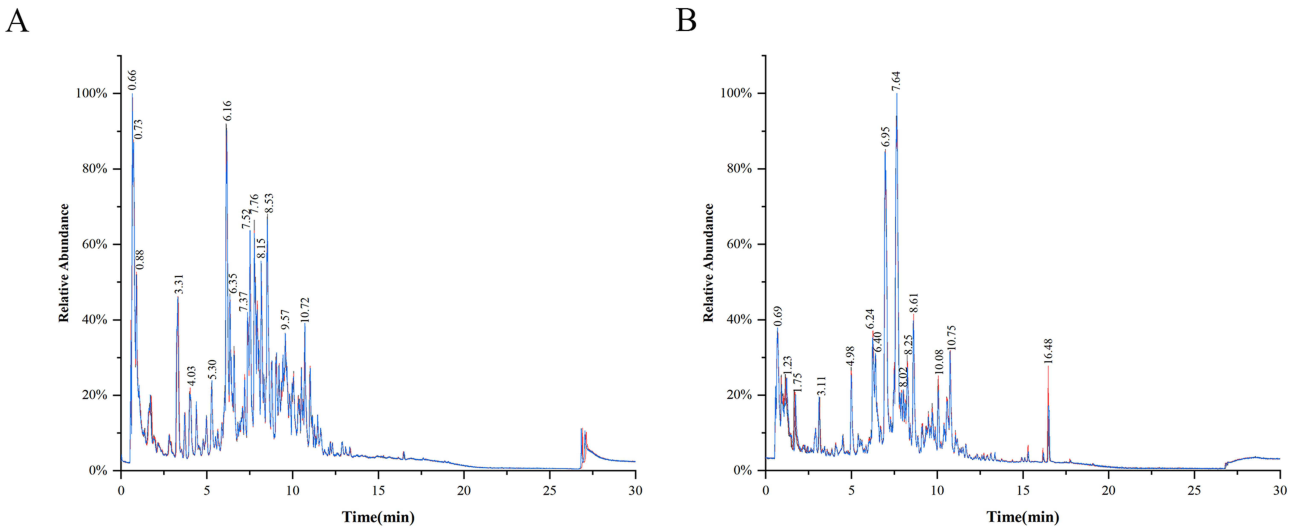

Figure 1 BPI chromatograms of BXD in positive (**A**) and negative (**B**) ionization modes.

BXD Alleviated the Symptoms of Colitis in CAC Mice

The therapeutic efficacy of BXD was assessed by evaluating multiple clinical and pathological parameters in a murine CAC model, including the DI and body weight (Figure 2A and B). Body weight was recorded throughout the experimental period. Compared with the control group, the model group showed a reduction in body weight. From day 28 onward, mice received

Table 3 Details of the 67 Main Metabolites in BXD

No.	Main metabolites	Formula	m/z	Retention Time (min)	Adducts	Peak Area
1	Gingerol	C17H26O4	275.90640	0.52	[M-H]-	1045195.52
2	Lysine	C6H14N2O2	147.11289	0.58	[M+H]+	22940730.65
3	Arginine	C6H14N4O2	175.11911	0.65	[M+H]+	5061837436.64
4	Trigonelline HCl	C7H7NO2.HCl	138.05499	0.69	[M+H]+	599364004.20
5	Cyclic AMP	C10H12N5O6P	330.05854	0.69	[M+H]+	146322783.50
6	Adenosine monophosphate	C10H14N5O7P	348.07126	0.88	[M+H]+	48871965.39
7	Valine	C5H11NO2	118.08661	0.90	[M+H]+	218600193.81
8	Uracil	C4H4N2O2	113.03493	0.94	[M+H]+	77360507.39
9	Uridine	C9H12N2O6	243.06236	0.96	[M-H]-	21819354.20
10	Guanine	C5H5N5O	152.05686	1.12	[M+H]+	805985559.40
11	4-Hydroxybenzoic acid	C7H6O3	137.02340	3.40	[M-H]-	50530769.71
12	Caffeic acid	C9H8O4	179.03445	4.24	[M-H]-	50821402.48
13	Isoleucine	C6H13NO2	132.10222	4.30	[M+H]+	8425548.05
14	Liquiritin	C21H22O9	417.11992	4.51	[M-H]-	303007247.01
15	Tetramethylcurcumin	C25H28O6	423.17844	4.97	[M-H]-	5984862.39
16	Vicenin II	C27H30O15	593.15115	5.05	[M-H]-	228290943.71
17	Liquiritigenin	C15H12O4	257.08081	6.14	[M+H]+	10431846438.88
18	Demethyleneberberine	$C19H18NO4^+$	324.12354	6.16	[M]+	759072368.49
19	Scutellarin	C21H18O12	463.08743	6.24	[M+H]+	720231557.85
20	Verbascoside	C29H36O15	642.24113	6.66	[M+NH4]+	113865532.71
21	Gingerenone A	C21H24O5	357.17044	7.35	[M+H]+	24785829.77
22	Berberrubine	C19H15NO4	322.10770	7.41	[M+H]+	896549459.13
23	Curcumin I	C23H24O6	397.16544	7.41	[M+H]+	5388077.53
24	Ginsenoside-Rg1	C42H72O14	845.49209	7.54	[M+FA]-	451968901.40
25	Ginsenoside Re	C48H82O18	945.54371	7.54	[M-H]-	11003910.94

(*Continued*)

Table 3 (Continued).

No.	Main metabolites	Formula	m/z	Retention Time (min)	Adducts	Peak Area
26	Baicalein	C15H10O5	269.04567	7.64	[M-H]-	319170594.10
27	Worenine	$C20H16NO4^+$	335.11284	7.65	[M+H]+	75111163.36
28	Ascorbic acid	C6H8O6	175.02403	7.67	[M-H]-	11273661.00
29	Ginsenoside Rc	C53H90O22	1123.59451	7.78	[M+FA]-	336,698.27
30	Ginsenoside Ro	C48H76O19	955.49227	7.86	[M-H]-	3362226.18
31	Wogonoside	C22H20O11	461.10893	7.96	[M+H]+	109423282.00
32	Isoliquiritin	C21H22O9	417.11992	7.97	[M-H]-	73471667.95
33	Licoricesaponin G2	C42H62O17	837.39556	8.08	[M-H]-	70192028.18
34	Ginsenoside F3	C41H70O13	815.48370	8.40	[M+FA]-	3413380.74
35	Ginsenoside Rh1	C36H62O9	683.43996	8.87	[M+FA]-	24851.24
36	Glycyrrhizin	C42H62O16	823.41346	8.89	[M+H]+	30572189.03
37	3'-O-Methylgancaonin P	C21H20O7	385.12871	8.97	[M+H]+	34242751.08
38	Baicalin methyl ester	C22H20O11	461.10902	9.10	[M+H]+	988003343.87
39	Ginsenoside La	C42H70O13	783.49091	9.12	[M+H]+	3723159.84
40	Licoricesaponin K2	C42H62O16	823.41378	9.18	[M+H]+	20239278.46
41	(S)-[10]-Gingerol	C21H34O4	351.25397	9.19	[M+H]+	24975596.10
42	Ginsenoside Rf	C42H72O14	799.48831	9.19	[M-H]-	31235394.49
43	Apigenin	C15H10O5	271.06027	9.20	[M+H]+	397857300.76
44	Curcumin	C21H20O6	369.13417	9.23	[M+H]+	43554677.49
45	Isoliquiritigenin	C15H12O4	255.06681	9.35	[M-H]-	8141169.52
46	Ginsenoside Rb2	C53H90O22	1077.58702	9.51	[M-H]-	41,899,569.14
47	Tetrahydrocurcumin	C21H24O6	371.15186	9.52	[M-H]-	41336441.62
48	Scutellarein	C15H10O6	285.04094	9.52	[M-H]-	18053677.04
49	Ginsenoside Rb3	C53H90O22	1123.59504	9.56	[M+FA]-	84879099.31
50	Oxyberberine	C20H17NO5	352.11891	9.65	[M+H]+	6272681.78
51	Methylgingerol	C18H28O4	307.19160	9.70	[M-H]-	4497650.72
52	Glabrolide	C30H44O4	469.33146	9.71	[M+H]+	1048809342.59
53	(20R)-Ginsenoside Rh1	C36H62O9	683.44050	9.75	[M+FA]-	27760659.38
54	Glycyrol	C21H18O6	367.12109	9.81	[M+H]+	44760135.54
55	Ginsenoside Rh3	C36H60O7	605.44118	9.95	[M+H]+	12910496.46
56	Baicalin	C21H18O11	445.07857	10.23	[M-H]-	18306670.99
57	Ginsenoside Rg6	C42H70O12	811.48552	10.80	[M+HCOO]-	9559978.22
58	Wogonin	C16H12O5	285.07634	11.09	[M+H]+	163729352.51
59	6-Gingerol	C17H26O4	293.17657	11.10	[M-H]-	1354987.07
60	Retrochalcone	C16H14O4	269.08236	11.10	[M-H]-	2806062.90
61	Ginsenoside Rg2	C42H72O13	783.49138	11.16	[M-H]-	8239644.33
62	[6]-Gingerdione	C17H24O4	293.17472	11.41	[M+H]+	10799352.75
63	Berberine	$C20H18NO4^+$	336.12367	11.52	[M+]	94543002.90
64	Ginsenoside F2	C42H72O13	829.49904	11.70	[M+FA]-	261634.39
65	Coptisine chloride	$C19H14NO4^+.Cl^-$	320.09243	12.74	[M]+	28109189.15
66	Jatrorrhizine	$C20H20NO4^+$	338.13880	16.54	[M]+	14717855.49
67	Palmatine chloride	$C21H22NO4^+.Cl^-$	352.15513	20.16	[M]+	6192185.07

Abbreviations: AOM/DSS, azoxymethane/dextran sulfate sodium salt; BP, biological process; BPI, base peak in-tensity; BXD, Banxia-Xiexin decoction; C3, complement C3; CAC, colitis-associated colorectal cancer; Cfh, complement factor H; CRC, colorectal cancer; DEMs, differential metabolites; DEPs, differentially expressed proteins; DI, disease index; Fgb, fibrinogen beta chain; Fgg, fibrinogen gamma chain; GO, gene ontology; HE, hematoxylin and eosin; KEGG, Kyoto Encyclopedia of Genes and Genomes; OPLS-DA, orthogonal partial least squares-discriminant analysis; PCA, principal components analysis; qRT-PCR, quantitative real-time polymerase chain reaction; ST, sulfasalazine tablets; TCM, traditional Chinese medicine.

varying doses of BXD or ST, leading to increases in both body weight gain across all treatment groups. In addition, all BXD groups and the ST group exhibited a significant decrease in DI compared with the model group.

Gross morphological examination of the colorectum at the endpoint (Figure 2C) revealed pronounced neoplastic hyperplasia in the Model group relative to Controls. In contrast, the BXDm and BXDh groups displayed substantial

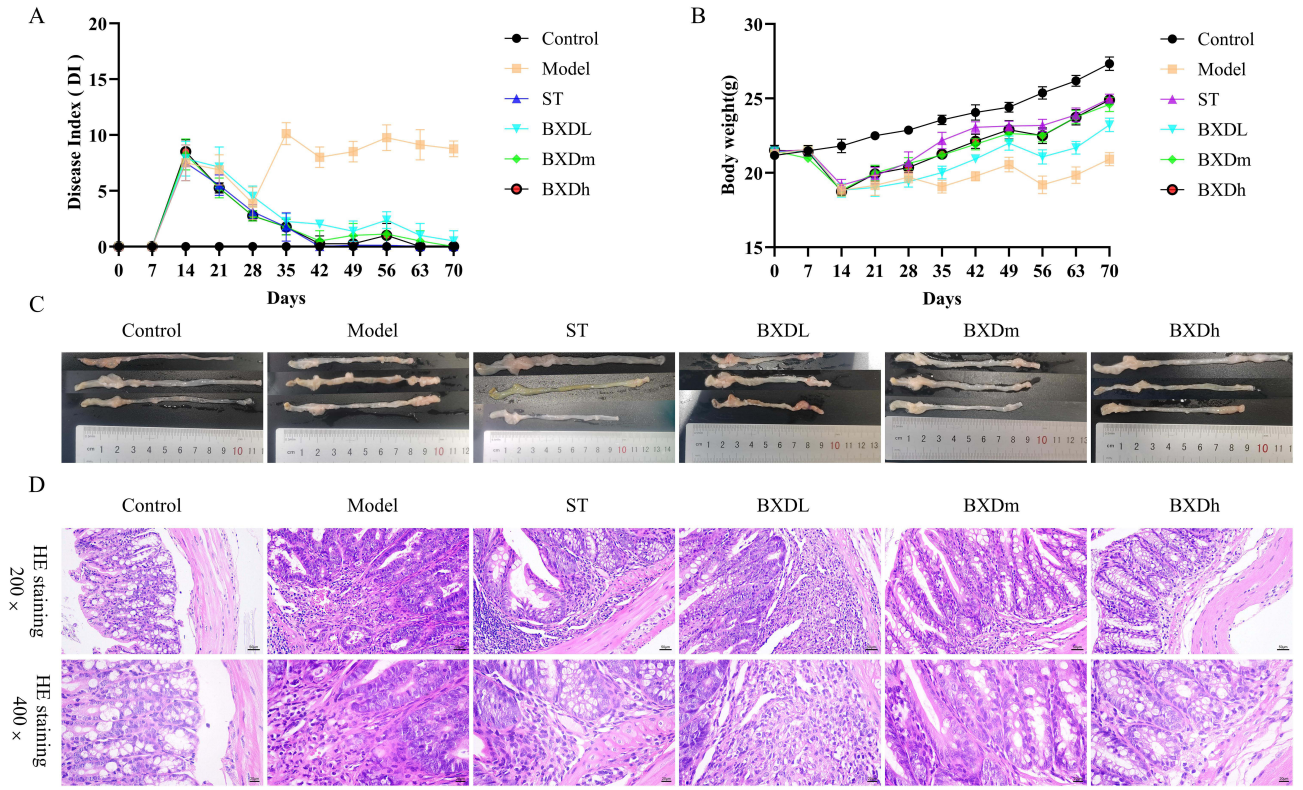

Figure 2 Effects of BXD on the pathological progress of CAC mice. (**A**) Effects of doses of BXD and ST on DI at different stages. (**B**) Effects of different doses of BXD and ST on body weight at different stages. (**C**) Colon and rectum morphology. (**D**) Pathological examination of mouse colon tissue.

reductions in tumor burden. Histopathological assessment by H&E staining (Figure 2D) showed severe pathological alterations in the Model group, including loss of crypt architecture, destruction of the mucosal layer, dense inflammatory cell infiltration, and malignant transformation. In the ST group, mild fibrous tissue proliferation and inflammatory infiltration were observed, with no evidence of malignancy. The BXDL group exhibited prominent fibrous tissue hyperplasia and inflammatory infiltration, but markedly fewer malignant lesions than the Model group. In the BXDm group, only mild crypt abnormalities and limited inflammation were detected without signs of malignancy. The BXDh group demonstrated increased crypt number, minimal inflammatory infiltration, and complete absence of malignant transformation.

BXD Reduced Pro-Inflammatory Cytokine Expression and Inflammatory Signaling Pathway Activation in CAC Mice

ELISA results showed that serum levels of the pro-inflammatory cytokines TNF-α, IL-6, IL-1β, and IFN-γ were markedly elevated in the model group compared with the control group (Figure 3A–D). BXD treatment significantly reduced serum concentrations of these cytokines relative to the model group. Immunofluorescence analysis further confirmed these findings. In colonic tissues, the expression of HIF-1α (Figure 3E), IFN-γ (Figure 3F), and NF-κB p65 (Figure 3G) was substantially higher in the model group than in controls, as evidenced by increased red fluorescence intensity. BXDh treatment markedly decreased the fluorescence intensity of all three proteins compared with the model group. These results indicate that BXD downregulated key inflammatory mediators and signaling pathways in the colon tissues of CAC mice.

BXD Partially Reversed Disorders of Serum Metabolism in CAC Mice

Serum metabolites were analyzed through an untargeted metabolomics approach. PCA revealed clear separation between the Control and Model groups, as well as between the Model and BXD groups, with tight clustering within each group (Figure 4A and B). To further resolve intergroup differences and identify potential biomarkers, supervised orthogonal

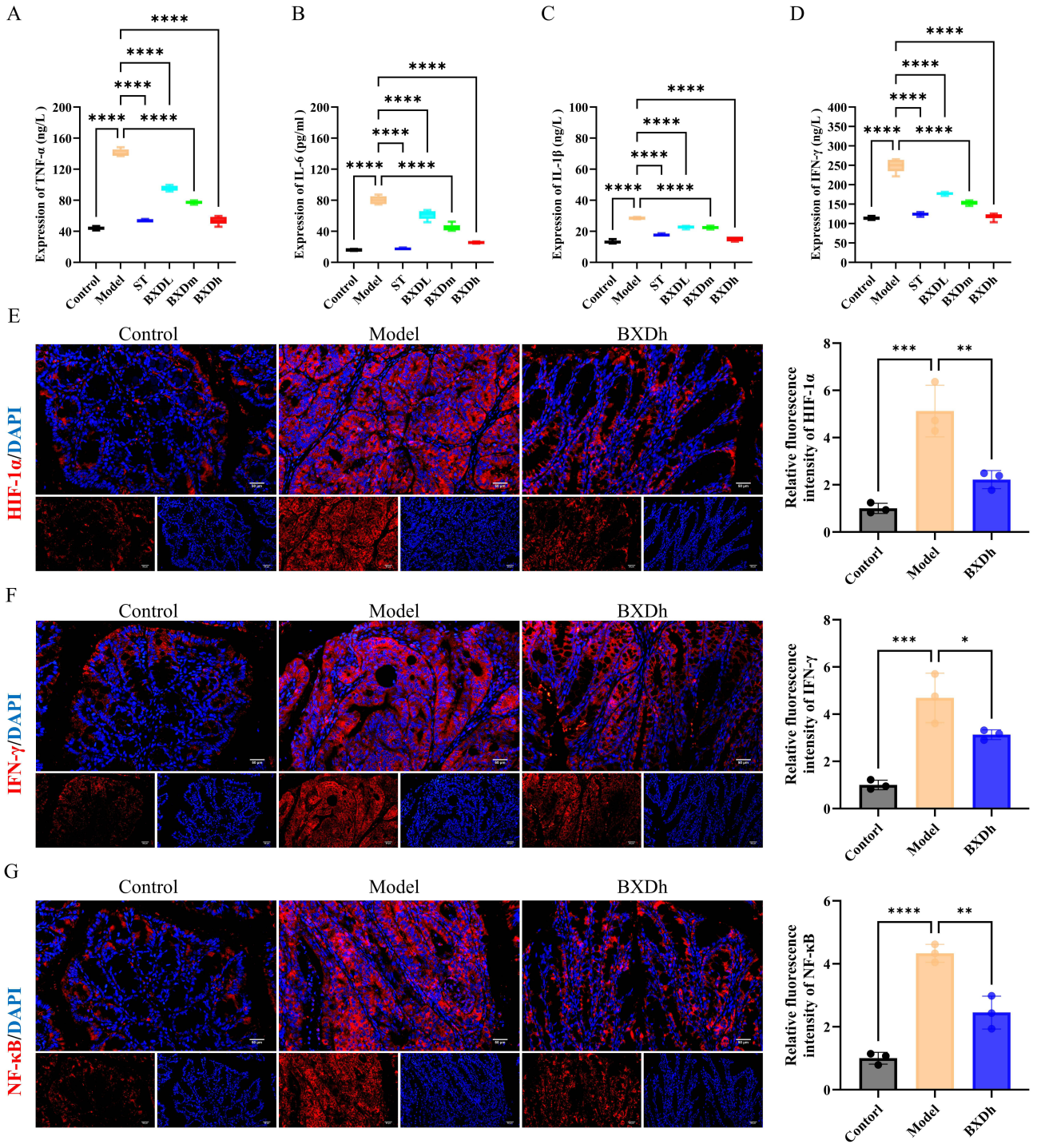

Figure 3 BXD reduced systemic and colonic inflammatory responses in CAC mice. (**A-D**) Serum levels of TNF-α, IL-6, IL-1β, and IFN-γ in each group (n = 8 per group). Compared with the model group, ****P < 0.0001. (**E-G**) Immunofluorescence assay for HIF-1α, IFN-γ and NF-κB (n = 3 per group). Compared with the model group, *P < 0.05, **P < 0.01, ***P < 0.001, ****P < 0.0001.

partial least squares discriminant analysis (OPLS–DA) was conducted. In both positive and negative ion modes, OPLS–DA scores demonstrated distinct segregation between Control and Model groups and between Model and BXD groups, indicating marked metabolic remodeling and good model discrimination (Figure 4C and D).

Differential metabolites were screened using the criteria |fold change (FC)| > 1, P < 0.05, and variable importance in projection (VIP) > 1.0. Volcano plots illustrated 541 significantly altered metabolites between the Model and Control groups,

https://doi.org/10.2147/JIR.S562302

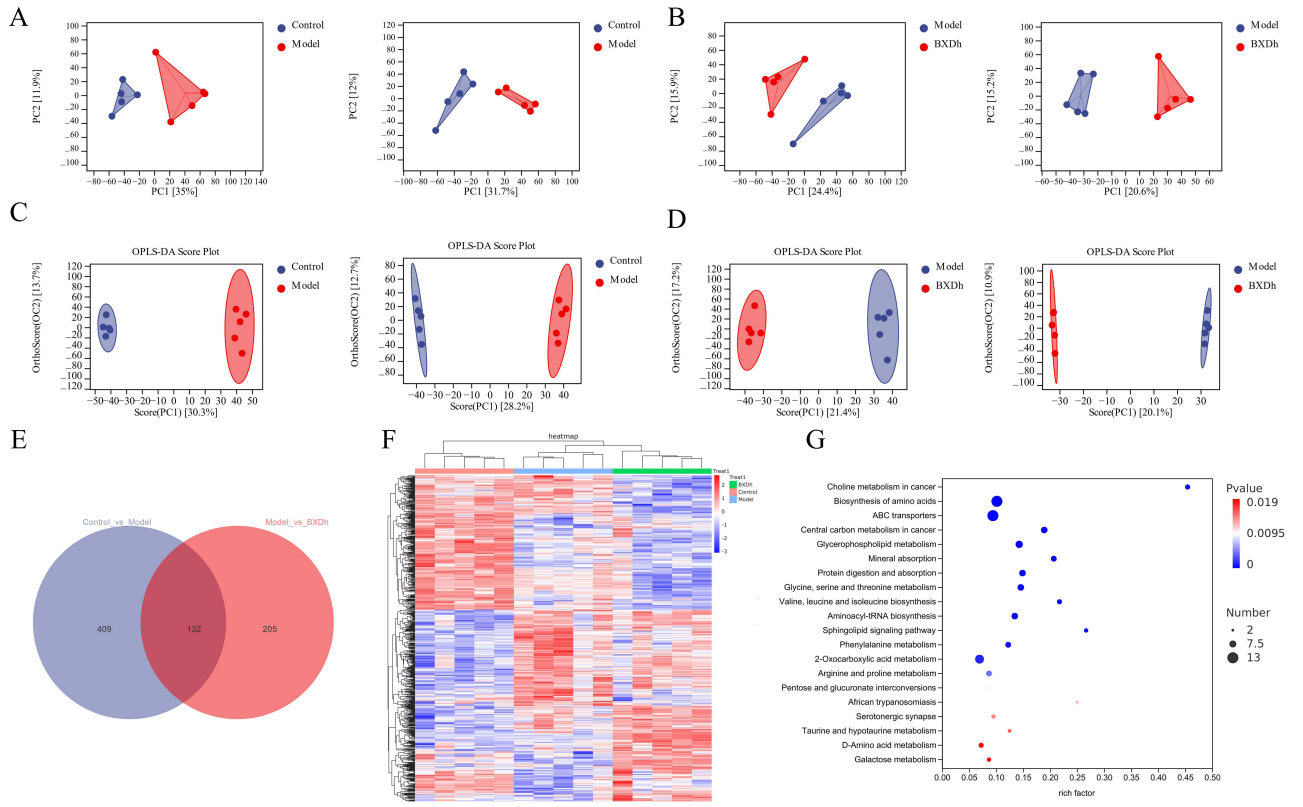

Figure 4 Changes in serum metabolomics in mice. (**A**) PCA between the control group and the model group in positive and negative ion modes. (**B**) PCA between the model group and the BXD group in positive and negative ion modes. (**C**) OPLS-DA between the control group and the model group in positive and negative ion modes. (**D**) OPLS-DA between the model group and the BXD group in positive and negative ion modes. (**E**) Venn diagram of DEMs. (**F**) Heatmap of DEMs. (**G**) KEGG pathway enrichment analysis of DEMs.

of which 273 were upregulated and 268 were downregulated (Figure S1A). Compared with the Model group, the BXD group showed 337 significantly altered metabolites, including 202 upregulated and 135 downregulated (Figure S1B). Further analysis using a Venn diagram revealed 132 differential metabolites that were consistently altered across all three groups, namely those significantly changed in each of the pairwise comparisons (Figure 4E). Hierarchical clustering based on the relative abundances of these differential metabolites (DEMs) distinctly separated samples from the control and model groups, highlighting pronounced metabolic differences. Notably, BXD treatment partially restored the altered metabolite profiles toward those observed in the control group (Figure 4F). Pathway enrichment analysis using the Kyoto Encyclopedia of Genes and Genomes (KEGG) database was performed for these DEMs. Pathways with $P < 0.05$ and an impact score > 0.1 were considered significantly enriched. The top 20 significantly affected pathways included central carbon metabolism in cancer, choline metabolism in cancer, amino acid biosynthesis, and glycerophospholipid metabolism (Figure 4G), highlighting the potential metabolic mechanisms underlying the therapeutic effects of BXD in CAC.

BXD Modulates Protein Expression Profiles in Colonic Tissue of CAC Mice

Label-free quantitative proteomic analysis identified a total of 8,949 proteins in colonic tissue. Comparative analysis between the Model and Control groups revealed 620 differentially expressed proteins (DEPs) (|fold change| > 1.5, $P < 0.05$), including 383 upregulated and 237 downregulated proteins in the Model group. In the BXD versus Model group comparison, 112 DEPs were detected, comprising 30 upregulated and 82 downregulated proteins (Figure 5A). Volcano plots illustrated clear distinctions in protein expression profiles between Model and Control groups (Figure 5B) and between BXD and Model groups (Figure 5C).

Hierarchical clustering of 34 overlapping DEPs from both comparisons revealed distinct expression patterns: the Model group exhibited a markedly altered protein profile, whereas the BXD group clustered more closely with the

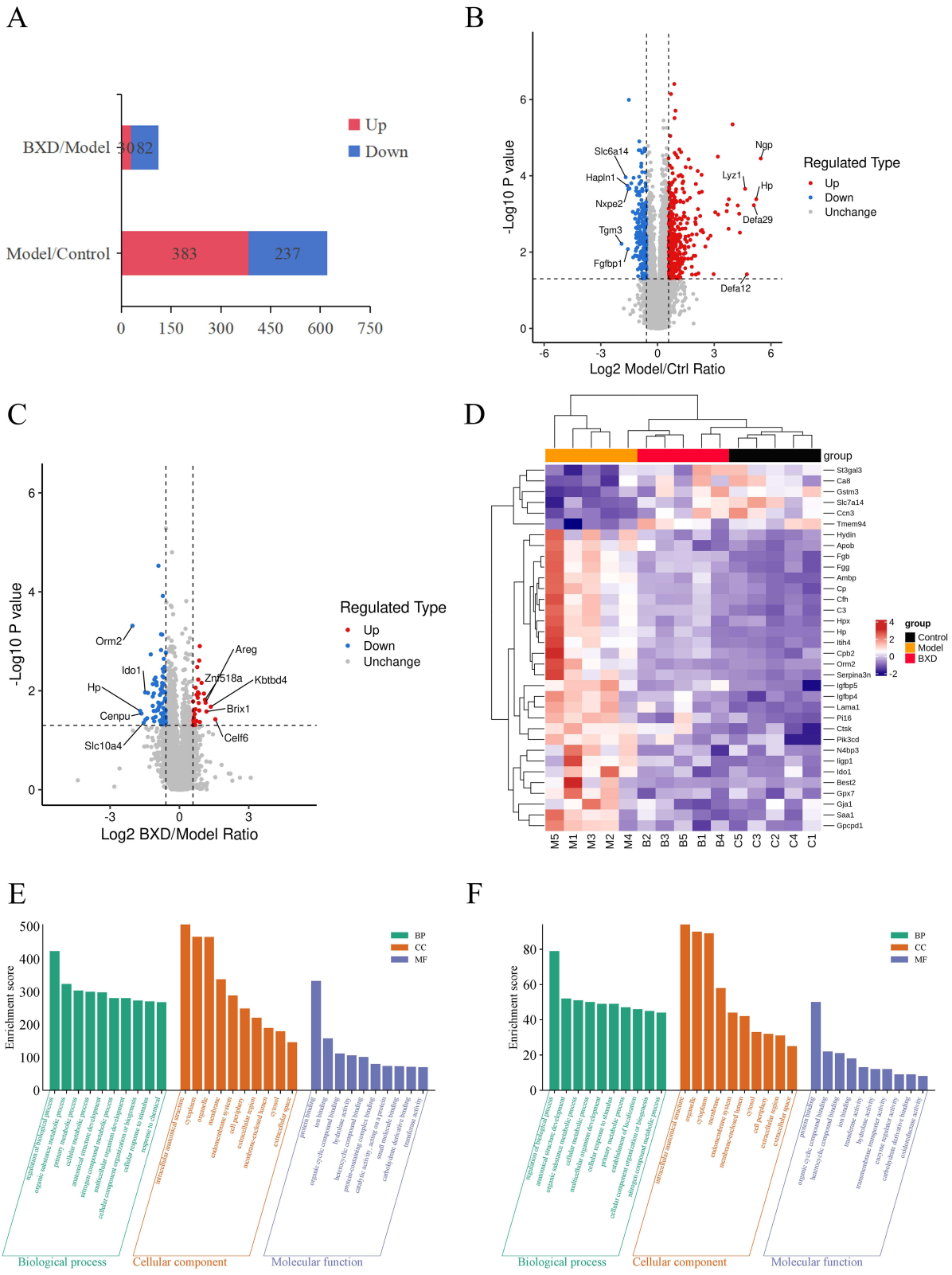

Figure 5 Differential protein expression profiles among Model, Control, and BXDh mice. (**A**) DEPs in BXDh/Model and Model/Control comparisons. (**B**) Statistical and volcano plots: Model vs Control group (**C**) Statistical and volcano plots: Model vs BXDh group (**D**) Heatmaps of DEPs (**E**) GO enrichment analysis of DEPs: Model vs Control group (**F**) GO enrichment analysis of DEPs: BXDh vs Model group.

https://doi.org/10.2147/JIR.S562302

Control group, indicating a restorative effect of BXD on protein dysregulation (Figure 5D). Notably, 28 proteins that were upregulated in the Model group were downregulated by BXD treatment, including fibrinogen gamma chain (Fgg), fibrinogen beta chain (Fgb), complement C3 (C3), and complement factor H (Cfh).

GO enrichment analysis was conducted to classify DEPs between the Model and Control groups, as well as between the BXDh and Model groups. In the model versus control comparison, DEPs were predominantly enriched in Biological Process (BP) terms such as regulation of biological processes and organic substance metabolic processes (Figure 5E). In contrast, BXD treatment modulated DEPs that were enriched in similar BP pathways, suggesting a partial reversal of the pathological proteomic alterations toward a more homeostatic state (Figure 5F).

KEGG pathway analysis revealed that DEPs between the BXDh group and the model group were significantly enriched in several pathways, with the most prominent being biosynthesis of unsaturated fatty acids, complement and coagulation cascades, and metabolism of xenobiotics by cytochrome P450 (Figure 6A and B). Notably, the complement and coagulation

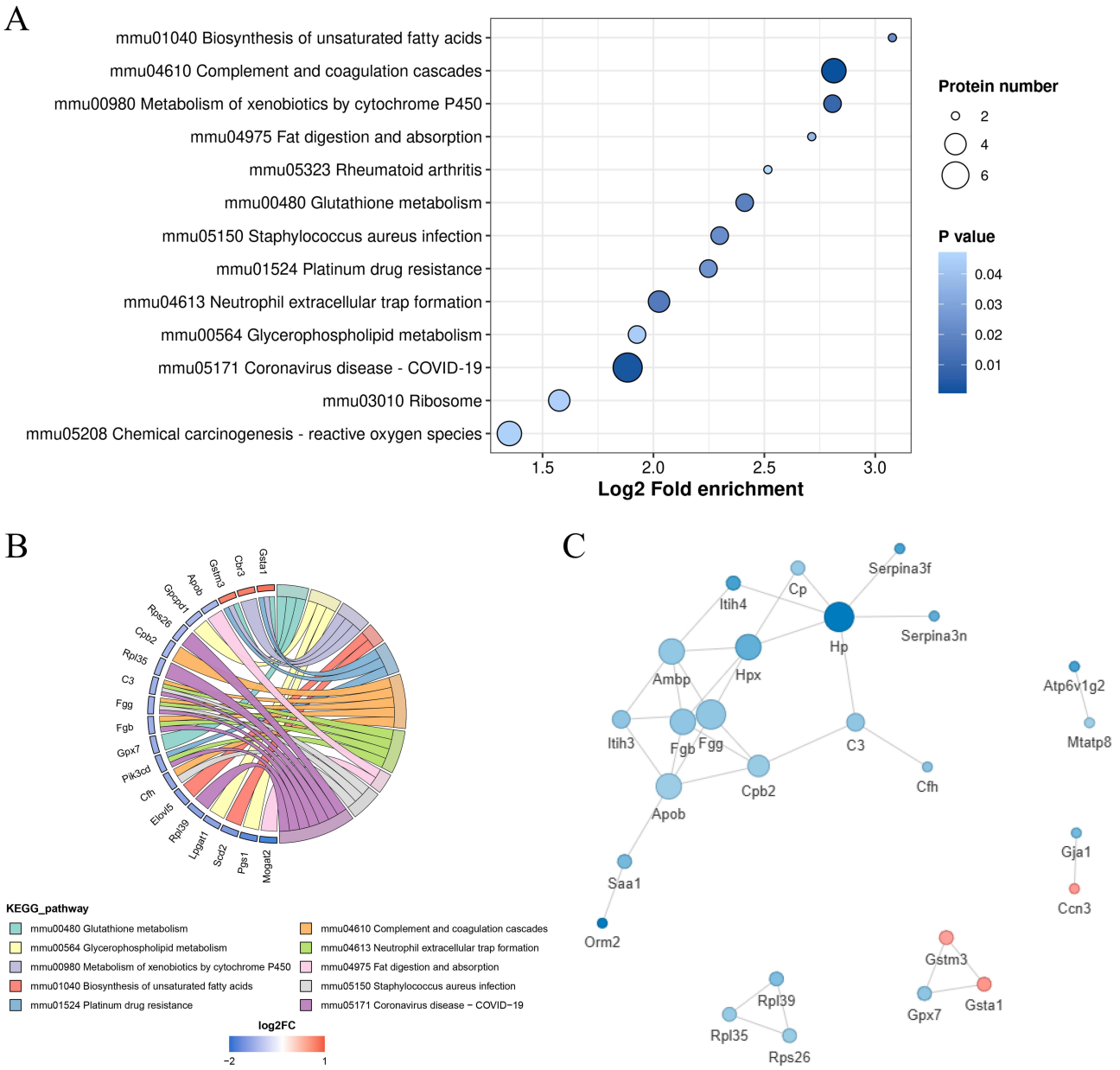

Figure 6 KEGG analyses of the BXDh group with Model group and the PPI networks (**A**) KEGG enrichment bubble chart of DEPs in the BXDh vs Model group. (**B**) KEGG enrichment string plot of DEPs in the BXDh vs Model group. (**C**) PPI network analysis in the BXDh vs Model group.

cascades pathway was also enriched in the comparison between the control and model groups (Figure S2), suggesting that dysregulation of this pathway may represent a core pathological feature of CAC. To further investigate the functional interactions among DEPs, a protein–protein interaction (PPI) network was constructed using STRING with a confidence score cutoff > 0.7 (Figure 6C). This network highlighted several highly interconnected nodes that may serve as critical mediators of BXD's protective effects.

Combined Analysis of Metabolomics and Proteomics

Integrated metabolomic and proteomic analysis was conducted to explore the molecular interactions underlying the therapeutic effects of BXD on CAC. Correlation analysis between DEPs and DEMs in the BXDh vs model comparison revealed multiple significant associations (Spearman correlation, $P < 0.05$). Notably, complement-related proteins (C3, Cfh, Cpb2, and Fgg) showed positive correlations with metabolite M696 [5-(5-hydroxy-3-(hydroxymethyl)pentyl)-8a-(hydroxymethyl)-5,6-dimethyl-3,4,4a,6,7,8-hexahydronaphthalene-1-carboxylic acid], and negative correlations with several branched-chain amino acid (BCAA) intermediates, including M28 (2-ketocaproic acid), M29 (3-methyl-2-oxo-valeric acid), and M30 (ketoleucine)(Figure 7A).

KEGG pathway enrichment analysis integrating proteomic and metabolomic datasets indicated significant enrichment in the complement and coagulation cascades pathway as well as D-Amino acid metabolism, Cholesterol metabolism, and Glycerophospholipid metabolism (Figure 7B and Figure S3). To validate these findings, qRT-PCR was performed on

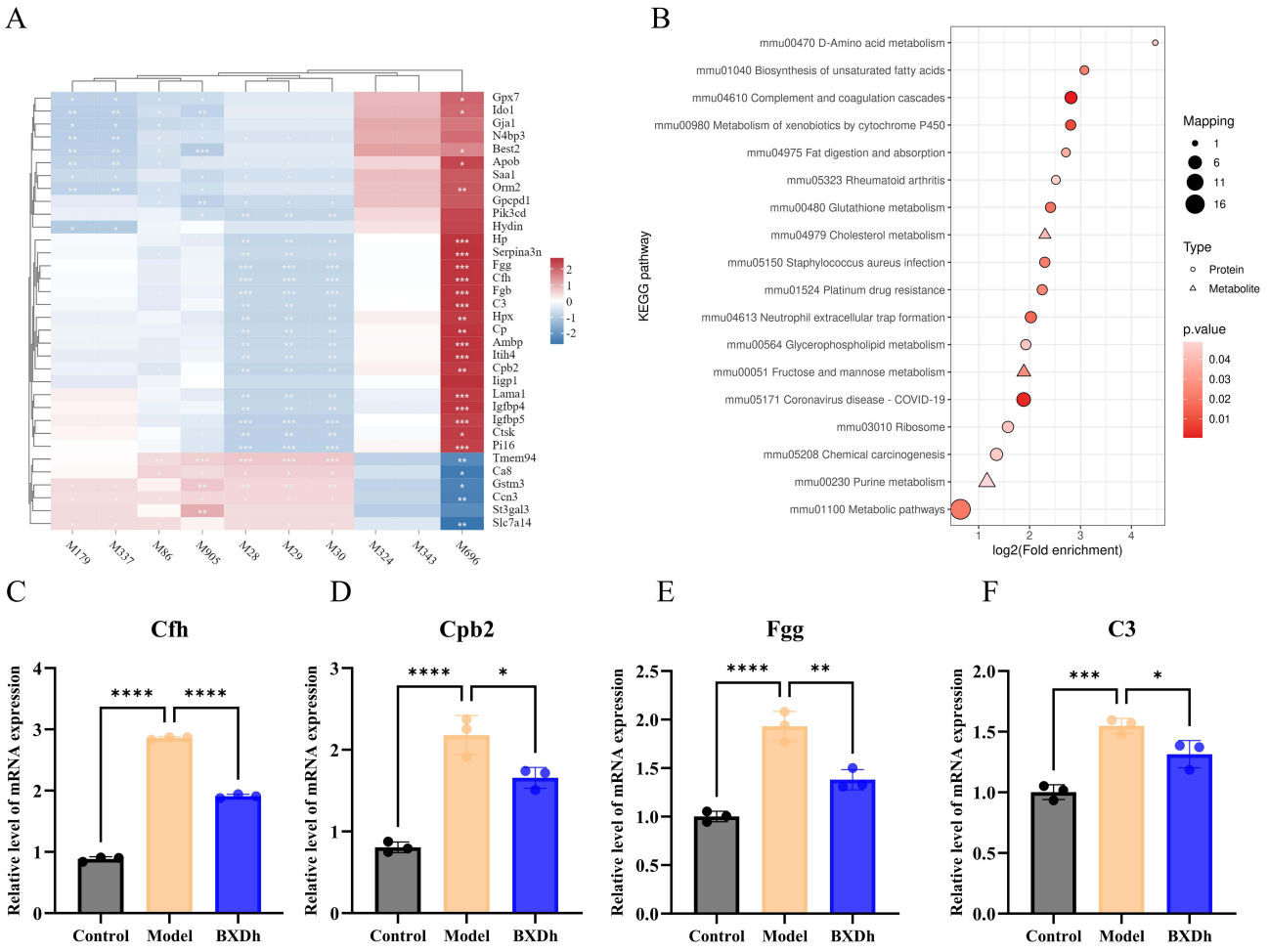

Figure 7 Combined metabolomics and proteomics analysis between the BXDh and model groups. (**A**) Correlation analysis between DEPs and DEMs in the BXDh vs model comparison. (**B**) KEGG pathway enrichment analysis based on integrated proteomic and metabolomic data (**C**) The mRNA expression of Cfh (n = 3 per group). (**D**) The mRNA expression of Cpb2 (n = 3 per group). (**E**) The mRNA expression of Fgg (n = 3 per group). (**F**) The mRNA expression of C3 (n = 3 per group). Compared with the model group, *P < 0.05, **P < 0.01, ***P < 0.001, ****P < 0.0001.

https://doi.org/10.2147/JIR.S562302

colonic tissues. mRNA expression levels of four key genes in the complement and coagulation cascades pathway—Cfh, Cpb2, Fgg, and C3—were significantly elevated in the Model group compared with Controls, whereas BXDh treatment markedly reduced their expression levels (Figure 7C–F). These results suggest that BXD may suppress CAC progression through modulation of the complement and coagulation cascades pathway.

Discussion

CAC is a distinct subtype of colorectal cancer that arises from chronic colonic inflammation and typically progresses through the "inflamed mucosa–dysplasia–carcinoma" sequence.[22] Chronic intestinal inflammation and persistent activation of oncogenic signaling pathways foster a tumor-supportive microenvironment, yet effective and safe pharmacological strategies remain scarce. In recent years, accumulating evidence has suggested that TCM may offer promising avenues for the prevention and treatment of CAC.[23] BXD, a classical TCM formula, is characterized by multi-component, multi-target, and multi-pathway synergistic effects, making it a promising candidate. However, the precise mechanisms underlying BXD's efficacy in CAC remain largely unclear, which hampers its broader clinical application.

In the present study, UHPLC-Q Exactive Orbitrap MS analysis identified 67 primary metabolites in BXD, 19 of which were quantified. Many of these bioactive compounds originate from the constituent herbs of BXD and possess reported anti-inflammatory and antineoplastic activities. For example, ginsenosides (Rg1, Rb2, Rb3, Rh3, Re, Rg2) from Panax ginseng have been shown to modulate gut microbiota, inhibit NF-κB and EGFR/SOX2 signaling, restore mucosal integrity, and suppress tumor cell proliferation.[24–27] Flavonoids such as wogonin, wogonoside, and baicalin from Scutellaria baicalensis can induce apoptosis, regulate PI3K/Akt/mTOR pathways, reinforce intestinal barrier function, and reduce proinflammatory cytokine levels.[28–31] Notably, several of these documented activities—particularly NF-κB inhibition and immune modulation—correspond well with the key regulatory pathways identified in our current study. Nevertheless, due to the considerable number of metabolites identified, comprehensive pharmacological validation of each compound was beyond the scope of the present work, which constitutes a limitation and highlights the need for future in-depth investigations.

In vivo, BXD treatment significantly improved the DI and reduced tumor burden in mice with CAC. HE staining further confirmed its therapeutic efficacy, demonstrating inhibition of colorectal tumor growth and attenuation of inflammatory cell infiltration. The pro-inflammatory cytokines TNF-α, IL-6, IL-1β, and IFN-γ are widely recognized as central mediators of chronic colonic inflammation and tumor progression in CAC.[32] The expression of these cytokines is primarily regulated by the NF-κB signaling pathway. The NF-κB pathway is a well-established regulator of both inflammatory responses and colonic tumorigenesis, orchestrating the transcription of numerous pro-inflammatory cytokines. Persistent NF-κB activation has been shown to promote the formation of a tumor-supportive microenvironment in CAC.[33] In the present study, BXD significantly reduced serum levels of TNF-α, IL-6, IL-1β, and IFN-γ in CAC mice, while also downregulating HIF-1α, IFN-γ, and NF-κB p65 expression in colonic tissues. These findings suggest that the therapeutic effects of BXD in CAC may be mediated through the suppression of pro-inflammatory cytokines by modulating the NF-κB signaling pathway.

Given the established bidirectional link between inflammation and tumor metabolism, we further applied non-targeted metabolomics to explore the metabolic basis of BXD's effects. Differentially expressed metabolites were primarily enriched in pathways such as biosynthesis of amino acids and glycerophospholipid metabolism, all of which are closely associated with inflammatory responses, immune regulation, and energy metabolism in tumor cells. These findings suggest that BXD treatment exerts a broad regulatory influence on cellular metabolism, characterized by the restoration of metabolic homeostasis and attenuation of tumor-associated metabolic reprogramming. By modulating these critical pathways, BXD may alleviate or reverse inflammation-driven metabolic disturbances in CAC. Previous studies suggest that targeted interventions in these pathways can substantially influence tumor metabolism and may even alter tumor growth and metastatic potential.[34,35]

To explore the multi-level mechanisms of BXD in the treatment of CAC, we performed an integrative analysis combining proteomics and metabolomics datasets. Correlation analysis revealed significant associations between differential metabolites and proteins. KEGG pathway enrichment analysis identified the complement and coagulation cascades as the most significantly enriched pathway. Dysregulation of the complement system has been reported to trigger pronounced inflammatory responses, promote tumor progression, and contribute to poor prognosis in colorectal and other cancers.[36,37] Therefore, inhibition of these pathways may be essential for effective CAC therapy. In our model, proteomics and qRT-PCR demonstrated that C3, fibrinogen chains (Fgg/Fgb), and regulatory components (Cfh, Cpb2) were elevated in untreated CAC and

concomitantly reduced by BXD. This coordinated suppression may reflect an upstream attenuation of complement activation tone and thrombin–fibrin signaling, potentially resulting in lower generation of the anaphylatoxins C3a and C5a and reduced engagement of their cognate receptors (C3aR/C5aR1). Such changes are consistent with the observed reductions in serum TNF-α, IL-6, IL-1β, and IFN-γ, as well as decreased colonic NF-κB p65 and HIF-1α. Concurrently, the decrease in fibrinogen chains may weaken fibrin deposition–driven platelet activation and integrin-mediated endothelial and leukocyte activation, processes that sustain a tumor-supportive niche.

Notably, glycerophospholipid metabolism was significantly enriched in both proteomic and metabolomic datasets. Mechanistically, activation of complement components—particularly generation of anaphylatoxins C3a and C5a—can induce phospholipase-mediated hydrolysis of membrane glycerophospholipids and release of arachidonic acid. Arachidonic acid serves as a precursor for pro-inflammatory eicosanoids, which amplify local inflammation and can engage pro-tumorigenic signaling.[38] Sustained dysregulation of glycerophospholipid metabolism can alter membrane lipid composition, thereby disrupting lipid signaling and cellular homeostasis, altering signal transduction dynamics, and promoting the establishment of a tumor-supportive microenvironment.[39] Therefore, BXD-mediated suppression of key complement components may help restore glycerophospholipid metabolic balance, reduce inflammatory response, and ultimately attenuate CAC progression.

Our findings highlight the complement–coagulation gateway—with C3 and fibrinogen chains (Fgg/Fgb) as tractable upstream effectors and Cfh/Cpb2 as co-regulated nodes—as a potential mechanistic target of BXD. Through coordinated modulation of inflammation- and metabolism-related pathways, BXD treatment appears to attenuate NF-κB–driven cytokine production, limit overactivation of complement and coagulation cascades, and help restore glycerophospholipid metabolic balance. These interconnected effects may collectively contribute to the observed protection against CAC. Although further validation is warranted, this integrative mechanism provides a plausible basis for the multitarget therapeutic potential of BXD in CAC.

Despite these promising findings, several limitations should be acknowledged. First, although integrated proteomic and metabolomic analyses revealed strong correlations between BXD treatment and modulation of the complement–coagulation–glycerophospholipid axis, these results remain associative and represent mechanistic hypotheses rather than definitive causal evidence. Targeted functional validation, such as pathway inhibition or gene-silencing experiments, will be necessary to confirm the specific roles of these pathways. Second, to facilitate translation into clinical practice, future research should include human studies and pharmacokinetic evaluations to further clarify the absorption, metabolism, and systemic bioavailability of BXD. These efforts will help substantiate the therapeutic potential and mechanistic basis of BXD in CAC prevention and treatment.

Conclusion

This study suggests that BXD exerts a protective effect against CAC by modulating multiple pathways involved in inflammation and metabolism, particularly through the attenuation of NF-κB-mediated pro-inflammatory cytokine production. Integrated proteomic and metabolomic analyses indicate that BXD may alleviate CAC progression by reducing excessive activation of the complement and coagulation cascades and by restoring glycerophospholipid metabolic balance. These findings provide new insights into the potential mechanisms underlying the anti-CAC activity of BXD and support its further investigation as a prospective therapeutic agent.

Data Sharing Statement

The raw proteomics data generated in this study have been deposited in the PRIDE repository (Project Accession: PXD065556). Additional data are available from the corresponding author upon reasonable request, subject to ethical and privacy considerations.

Author Contributions

Qiang Chen: Conceptualization, Investigation, Data Curation, Writing – Original Draft, Visualization.

Maoxu Wang: Validation, Data Curation, Writing – Original Draft.

Wei Shi: Methodology, Investigation.

Yinan Liu: Investigation, Formal analysis.

Liying Wang: Investigation, Methodology, Software.

Yuegang Zhao: Validation, Software.

Zhidong Qiu: Supervision, Resources.

Ye Qiu: Methodology.

Xuelian Dong: Methodology, Conceptualization, Project administration, Writing – Review & Editing, Funding Acquisition.

All authors took part in drafting, revising or critically reviewing the article; gave final approval of the version to be published; have agreed on the journal to which the article has been submitted; and agree to be accountable for all aspects of the work.

Funding

This study was supported by the Jilin Province Science and Technology Development Plan, grant number 20220204002YY.

Disclosure

The authors report there are no competing interests to declare. We confirm that the design, conduct, and reporting of this study adhere to the ARRIVE guidelines, and a completed checklist is included as supplementary material.[40]

References

1. Rubin DT, Ananthakrishnan AN, Siegel CA, Sauer BG, Long MD. ACG clinical guideline: ulcerative colitis in adults. *Am J Gastroenterol*. 2019;114(3):384–413. doi:10.14309/ajg.0000000000000152
2. Dan WY, Zhou GZ, Peng LH, Pan F. Update and latest advances in mechanisms and management of colitis-associated colorectal cancer. *World J Gastrointestinal Oncol*. 2023;15(8):1317–1331. doi:10.4251/wjgo.v15.i8.1317
3. Hirano T, Hirayama D, Wagatsuma K, Yamakawa T, Yokoyama Y, Nakase H. Immunological mechanisms in inflammation-associated colon carcinogenesis. *Int J Mol Sci*. 2020;21(9):3062. doi:10.3390/ijms21093062
4. Wang Z, Chang Y, Sun HB, Li YQ, Tang TY. Advances in molecular mechanisms of inflammatory bowel disease-associated colorectal cancer (Review). *Oncol Lett*. 2024;27(6):257. doi:10.3892/ol.2024.14390
5. Liu L, Yang M, Dong WX, et al. Gut dysbiosis and abnormal bile acid metabolism in colitis-associated cancer. *Gastroenterol Res Pract*. 2021:20216645970. doi:10.1155/2021/6645970
6. Shah SC, Itzkowitz SH. Colorectal cancer in inflammatory bowel disease: mechanisms and management. *Gastroenterology*. 2022;162(3):715. doi:10.1053/j.gastro.2021.10.035
7. Irrazabal T, Thakur BK, Croitoru K, Martin A. Preventing colitis-associated colon cancer with antioxidants: a systematic review. *CMGH*. 2021;11(4):1177–1197. doi:10.1016/j.jcmgh.2020.12.013
8. Zhang ZY, Chen YX, Zheng YJ, et al. Quxie capsule alleviates colitis-associated colorectal cancer through modulating the gut Microbiota and suppressing *A. fumigatus*-induced aerobic glycolysis. *Integr Cancer Ther*. 2022;21. doi:10.1177/15347354221138534
9. Cheng Y, Li JX, Zhang XS, et al. Protective effect of Qingchang Wenzhong decoction on colitis and colitis-related carcinogenesis by regulating inflammation and intestinal fibrosis. *J Inflamm Res*. 2023;16:1479–1495. doi:10.2147/jir.S402395
10. Zhang YF, Zhang YQ, Zhao Y, et al. Protection against ulcerative colitis and colorectal cancer by evodiamine via anti-inflammatory effects. *Mol Med Rep*. 2022;25(5):188. doi:10.3892/mmr.2022.12704
11. Fabian O, Bajer L, Drastich P, et al. A current state of proteomics in adult and pediatric inflammatory bowel diseases: a systematic search and review. *Int J Mol Sci*. 2023;24(11):9386. doi:10.3390/ijms24119386
12. Li LZ, Liu HH, Yu JQ, et al. Intestinal microbiota and metabolomics reveal the role of *Auricularia delicate* in regulating colitis-associated colorectal cancer. *Nutrients*. 2023;15(23):5011. doi:10.3390/nu15235011
13. Zhou Z, An R, You L, Liang K, Wang X. Banxia Xiexin decoction A review on phytochemical, pharmacological, clinical and pharmacokinetic investigations. *Medicine*. 2023;102(35):e34891. doi:10.1097/md.0000000000034891
14. Liu JL, Huang JK, Zhang BH, et al. Treatment of the gastroesophageal reflux disease with Chinese herbal medicine (BanxiaXiexin Decoction): evidence from meta-analysis. *Evid Based Complement Alternat Med*. 2022:20221500660. doi:10.1155/2022/1500660
15. Wang XW, Yang JH, Cao Q, Tang JM. Therapeutic efficacy and mechanism of water-soluble extracts of Banxiaxiexin decoction on BALB/c mice with oxazolone-induced colitis. *Exp Ther Med*. 2014;8(4):1201–1204. doi:10.3892/etm.2014.1890
16. Wang Y, Zhao T, Huang CY, et al. Effect and mechanism of Banxia Xiexin decoction in colorectal cancer: a network pharmacology approach. *Phytomedicine*. 2024:123155174. doi:10.1016/j.phymed.2023.155174
17. Luo YT, Fu S, Liu YL, et al. Banxia Xiexin decoction modulates gut microbiota and gut microbiota metabolism to alleviate DSS-induced ulcerative colitis. *J Ethnopharmacol*. 2024:326117990. doi:10.1016/j.jep.2024.117990
18. Liao XX, Hu K, Xie XH, et al. Banxia Xiexin decoction alleviates AS co-depression disease by regulating the gut microbiome-lipid metabolic axis. *J Ethnopharmacol*. 2023:313116468. doi:10.1016/j.jep.2023.116468
19. Zhang R, Zhang QQ, Chen YN, et al. Combined treatment with Rg1 and adipose-derived stem cells alleviates DSS-induced colitis in a mouse model. *Stem Cell Res Ther*. 2022;13(1):272. doi:10.1186/s13287-022-02940-x

20. Zhang TH, Yuan KT, Wang YZ, et al. Identification of candidate biomarkers and prognostic analysis in colorectal cancer liver metastases. *Front Oncol*. 2021:11652354. doi:10.3389/fonc.2021.652354
21. Zhang JY, Chen CY, Yan W, Fu Y. New sights of immunometabolism and agent progress in colitis associated colorectal cancer. *Front Pharmacol*. 2024;141303913. doi:10.3389/fphar.2023.1303913
22. Jin XH, You LK, Qiao JC, Han WD, Pan HM. Autophagy in colitis-associated colon cancer: exploring its potential role in reducing initiation and preventing IBD-Related CAC development. *Autophagy*. 2024;20(2):242–258. doi:10.1080/15548627.2023.2259214
23. Wei XA, Leng XH, Li GY, Wang RT, Chi LL, Sun DJ. Advances in research on the effectiveness and mechanism of Traditional Chinese Medicine formulas for colitis-associated colorectal cancer. *Front Pharmacol*. 2023;141120672. doi:10.3389/fphar.2023.1120672
24. Cheng H, Liu J, Zhang DD, et al. Ginsenoside Rg1 alleviates acute ulcerative colitis by modulating gut microbiota and microbial tryptophan metabolism. *Front Immunol*. 2022:13817600. doi:10.3389/fimmu.2022.817600
25. Qian JN, Jiang YY, Hu HY. Ginsenosides: an immunomodulator for the treatment of colorectal cancer. *Front Pharmacol*. 2024;151408993. doi:10.3389/fphar.2024.1408993
26. Huang GX, Khan I, Li XA, et al. Ginsenosides Rb3 and Rd reduce polyps formation while reinstate the dysbiotic gut microbiota and the intestinal microenvironment in $Apc^{Min/+}$ mice. *Sci Rep*. 2017:712552. doi:10.1038/s41598-017-12644-5
27. Ni BY, Song XT, Shi BL, et al. Research progress of ginseng in the treatment of gastrointestinal cancers. *Front Pharmacol*. 2022:131036498. doi:10.3389/fphar.2022.1036498
28. Feng Q, Wang HJ, Pang JY, et al. Prevention of Wogonin on colorectal cancer tumorigenesis by regulating p53 nuclear translocation. *Front Pharmacol*. 2018:91356. doi:10.3389/fphar.2018.01356
29. Sun Y, Zhao Y, Wang XP, et al. Wogonoside prevents colitis-associated colorectal carcinogenesis and colon cancer progression in inflammation-related microenvironment via inhibiting NF-κB activation through PI3K/Akt pathway. *Oncotarget*. 2016;7(23):34300–34315. doi:10.18632/oncotarget.8815
30. Han CZ, Xing GZ, Zhang MY, et al. Wogonoside inhibits cell growth and induces mitochondrial-mediated autophagy-related apoptosis in human colon cancer cells through the PI3K/AKT/mTOR/p70S6K signaling pathway. *Oncol Lett*. 2018;15(4):4463–4470. doi:10.3892/ol.2018.7852
31. Li YA, Hu JY, Cheng C, et al. Baicalin ameliorates DSS-induced colitis by protecting goblet cells through activating NLRP6 inflammasomes. *Evid Based Complement Alternat Med*. 2022:20222818136. doi:10.1155/2022/2818136
32. Nardone OM, Zammarchi I, Santacroce G, Ghosh S, Iacucci M. Inflammation-driven colorectal cancer associated with colitis: from pathogenesis to changing therapy. *Cancers*. 2023;15(8):2389. doi:10.3390/cancers15082389
33. Yan SH, Chang JY, Hao XH, et al. Berberine regulates short-chain fatty acid metabolism and alleviates the colitis-associated colorectal tumorigenesis through remodeling intestinal flora. *Phytomedicine*. 2022:102154217. doi:10.1016/j.phymed.2022.154217
34. Liu MX, Yang CJ, Peng XJ, et al. Formononetin suppresses colitis-associated colon cancer by targeting lipid synthesis and mTORC2/Akt signaling. *Phytomedicine*. 2025:142156665. doi:10.1016/j.phymed.2025.156665
35. Wang DF, Zhu L, Liu HF, et al. Huangqin tang alleviates colitis-associated colorectal cancer via amino acids homeostasisand PI3K/AKT/mtor pathway modulation. *J Ethnopharmacol*. 2024:334118597. doi:10.1016/j.jep.2024.118597
36. O'Brien RM, Cannon A, Reynolds JV, Lysaght J, Lynam-Lennon N. Complement in tumourigenesis and the response to cancer therapy. *Cancers*. 2021;13(6):1209. doi:10.3390/cancers13061209
37. Azoulay E, Zuber J, Bousfiha AA, et al. Complement system activation: bridging physiology, pathophysiology, and therapy. *Intensive Care Med*. 2024;50(11):1791–1803. doi:10.1007/s00134-024-07611-4
38. Pan PL, Qin GD, Wang B, et al. HDAC5 loss enhances phospholipid-derived arachidonic acid generation and confers sensitivity to cPLA2 inhibition in pancreatic cancer. *Cancer Res*. 2022;82(24):4542–4554. doi:10.1158/0008-5472.Can-21-4362
39. Cheng Q, Na K, Xu CS, et al. Untargeted metabolomics reveals the inhibition effect of a high-fat diet on colorectal cancer tumorigenesis in obesity-resistant mice *via* regulating bile acid, glutathione, and glycerophospholipid metabolisms. *Food Funct*. 2025;16(13):5526–5542. doi:10.1039/d4fo06132b
40. du Sert N P, Hurst V, Ahluwalia A, et al. The ARRIVE guidelines 2.0: updated guidelines for reporting animal research. *PLoS Biol*. 2020;18(7):e3000410. doi:10.1371/journal.pbio.3000410